Compact TDLAS based optical sensor for ppb-level ethane detection by use of a 3.34 µm room-temperature CW interband cascade laser

Chunguang Li[a,b], Lei Dong[a,c,*], Chuantao Zheng[a,b], Frank K. Tittel[a,**]

[a] Department of Electrical and Computer Engineering, Rice University, 6100 Main Street, Houston, TX 77005, USA

[b] State Key Laboratory on Integrated Optoelectronics, College of Electronic Science and Engineering, Jilin University, Changchun 130012, China

[c] State Key Laboratory of Quantum Optics and Quantum Optics Devices, Institute of Laser Spectroscopy, Shanxi University, Taiyuan 030006, China

[*] donglei@sxu.edu.cn

[**] fkt@rice.edu

Abstract

A mid-infrared ethane (C_2H_6) sensor based on a wavelength modulation spectroscopy (WMS) technique was developed using a thermoelectrically cooled (TEC), continuous-wave (CW) interband cascade laser (ICL) emitting at 3.34 µm and a dense multi-pass gas cell (MPGC, 17 × 6.5 × 5.5 cm3) with a 54.6 m optical path length. A compact optical sensor system with a physical size of 35.5 × 18 × 12.5 cm^3 was designed and constructed. An ICL was employed for targeting a strong C_2H_6 line at 2996.88 cm^{-1} at <100 Torr gas pressure in the fundamental absorption band of C_2H_6. The sensor performance, including the minimum detection limit (MDL) and the stability were improved by reducing the effect of laser power drift by means of the 2*f*/1*f*-WMS technique. A MDL of ~1.2 parts per billion (ppbv) for 2f-WMS and ~1.0 ppbv for 2*f*/1*f*-WMS were achieved, respectively, with a measurement time of 4 s. The MDL was further improved from 299 pptv (@108 s for 2*f*-WMS) to 239 pptv (@208 s for 2*f*/1*f*-WMS), based on an Allan deviation analysis. The rise time (@0 → 100 ppbv) and fall time (@100 → 0 ppbv) were determined to be ~64 s and ~48 s, respectively, at a gas pressure of <100 Torr for the C_2H_6 sensor operation.

1. Introduction

Ethane (C_2H_6) is the second-largest component of natural gas after methane (CH_4) and is used in the chemical industry in the production of ethylene (C_2H_4) or as a feedstock in the manufacture of other commodity chemicals. C_2H_6 is a combustible gas at room temperature and is explosive when it is mixed with 3–12.5% volume of air. C_2H_6 occurs as a trace gas in the earth's atmosphere, at concentration levels of several ppbv, although its pre-industrial concentration levels were lower since a significant proportion of the ethane in the atmosphere originates from fossil fuels. Hence, as one of the most abundant nonmethane hydrocarbons in the atmosphere at ppbv concentration level, C_2H_6 influences both atmospheric chemistry and climate [1,2], and is therefore an important gas in environmental monitoring [3,4]. Furthermore, ultra-sensitive C_2H_6 detection has also found applications in human breath analysis as a non-invasive method to monitor and identify diseases, such as lung cancer, asthma, by the detection of C_2H_6 concentrations in exhaled human breath [5–7].

Infrared tunable direct laser absorption spectroscopy (TDLAS) [8–10] enables non-contact trace gas measurements, and has proven to be an excellent tool for sensitive and selective detection in environmental [11–13], biomedical [14–20], industrial [21,22] and national security [13] applications. TDLAS requires a tunable laser exhibiting single frequency emission and a narrow linewidth at the targeted absorption line of a gas molecule in order to achieve high detection sensitivity and selectivity in the mid-infrared spectral range. Commercially available laser sources generally include semiconductor lasers, difference-frequency generation (DFG) [23], optical parametric oscillators (OPOs) [24] in the past, but in recent years quantum cascaded lasers (QCLs) [25] in the 3.7–12 µm spectral range and interband cascaded lasers (ICLs) in the 3–6 µm spectral range with low power-consumption [26] provide advantages in terms of continuous-wave (CW), distributed feedback (DFB) output power levels (up to hundreds of mW for QCLs and tens of mW for ICLs) and compactness. C_2H_6 has strong absorption features in the 3–4 µm spectral region where its fundamental absorption band is located. C_2H_6 detection with high precision and sensitivity takes advantage of a line strength of several orders of magnitude stronger than in the near infrared overtone absorption band. A mid-infrared C_2H_6 absorption spectrometer using a TEC, DFB diode laser and a 57.6 m optical path-length multipass gas cell (MPGC) was reported in Ref. [27]. C_2H_6 measurements with a minimum detection limit (MDL) of 740 pptv were achieved at ~3.36 µm with a 1 s integration time. Furthermore C_2H_6 measurements based on a CW, thermoelectrically cooled (TEC), DFB laser diode were performed with a 100 m optical path length astigmatic Herriott cell and a MDL of 240 pptv with a 1 s integration time was obtained [28]. Although these sensor systems achieved ppt detection sensitivities, they were too large to be suitable and convenient for some applications such as in field measurements (eg. mobile and airborne).

In this work, a compact C_2H_6 sensor system based on a compact MPGC with a physical size of $35.5 \times 18 \times 12.5$ cm^3 and a 54.6 m absorption length was employed. A TEC, CW, DFB, ICL centered at 2996.88 cm^{-1} from Nanoplus (Germany) was used as the excitation source. The optical components were mounted on an aluminum plate, which provided good mechanical stability for sensing performance. Both 2*f*-wavelength modulation spectroscopy (WMS) and 2*f*/1*f*-WMS [29,30] techniques were adopted in the reported sensor system, and the latter technique was shown to be more stable for field applications.

2. Sensor configuration and optimization

2.1. Optimum C_2H_6 line selection

Most atmospheric trace gas species have strong fundamental absorption band in the mid-infrared spectral range, which facilitates the sensitive and selective detection of atmospheric trace gases in this spectral range. Ethane has a strong absorption band located at 3.34 µm. At this wavelength, the potential spectral interferences mainly originate from methane (CH_4) and water (H_2O), which will affect the C_2H_6 detection. High-resolution transmission molecular absorption database (HITRAN) is a worldwide standard for calculating or simulating atmospheric molecular transmission and radiation, which covers a wide spectral region from the microwave to the ultraviolet [31]. HITRAN absorption spectra of 10 ppb

C_2H_6, 1.8 ppm CH_4, and 2% H_2O at a 100 Torr gas pressure and a 54.6 m effective optical path length are depicted in Fig. 1. A C_2H_6 absorption line centered at 3336.8 nm (2996.88 cm^{-1}) was selected as the optimum C_2H_6 target line. All the H_2O absorption lines (the two closest lines are located at 2996.4 cm^{-1} and 2997.3 cm^{-1}) under an absolute humidity of 2% do not interfere with the selected C_2H_6 line at 2996.88 cm^{-1}, since they are ~ 0.5 cm^{-1} away. With a higher relative humidity, the dryers can be used to lower the H_2O concentration and thereby reduce the absolute humidity to an acceptable level, e.g. below 2%. In that case, the sensor can operate normally. Besides H_2O lines, a weak CH_4 absorption line at 2997 cm^{-1} is observed in the presence of 10 ppb C_2H_6, and the spacing between the two lines is ~0.12 cm-1 at a pressure of ~100 Torr and a concentration of 1.8 ppm (i.e. the atmospheric concentration level). When the pressures is < 100 Torr, the 2997 cm^{-1} CH_4 line causes no interference to the C_2H_6 line. However, the C_2H_6 absorption line interferes once the pressure exceeds 150 Torr. Hence the pressure inside the MPGC must be <150 Torr in order to avoid over-lapping of the CH_4 and C_2H_6 absorption lines.

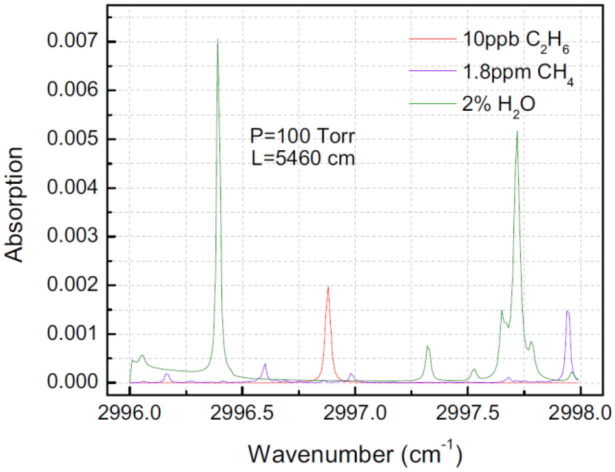

Figure 1. HITRAN based absorption spectra of C_2H_6 (10 ppbv), CH_4 (1.8 ppmv), and H_2O (2%) in a narrow spectral range from 2996 cm^{-1} to 2998 cm^{-1} for a 5460 cm path length at a pressure of 100 Torr. C_2H_6, CH_4, and H_2O lines are shown in red, purple, and green, respectively.

2.2. Sensor design

The C_2H_6 sensor architecture is depicted in Fig. 2(a), which includes both the optical and electrical sub-systems. In the optical part, a Nanoplus CW, DFB, TEC ICL was used as the excitation source and which is mounted in a TO66 header. The compact MPGC consists of two concave spherical mirrors capable of a novel, dense spot pattern, as shown in the insert of Fig. 2(b). Such a novel MPGC design offers a 54.6 m optical path length in a physical size of 17 × 6.5 × 5.5 cm^3 with a 220 mL sampling volume and results in a sensor platform that is more than 10 times smaller than conventional designs with equivalent sensitivity. In order to track the ICL beam, a dichroic mirror (ISP Optics, model BSP-DI-25-3) was used to combine a red alignment diode laser beam with the mid-infrared ICL beam. The combined laser beams were then coupled to the MPGC using a mid-IR transmitting CaF_2 lens (d = 25 mm, f = 200 mm) and two adjustable plane mirrors (M1 and M2). The ICL beam enters the gas cell at the designed position and angle in order to achieve the 453 reflections of the ICL beam before exiting the MPGC. The output beam is then focused onto a TEC mercury-cadmium-telluride (MCT) photodetector (VIGO System, model PVI-4TE-3.4) using a parabolic mirror (PM, d = 25 mm, f = 35 mm). The optical elements were mounted on an aluminum plate, as shown in the photo in Fig. 2(b).

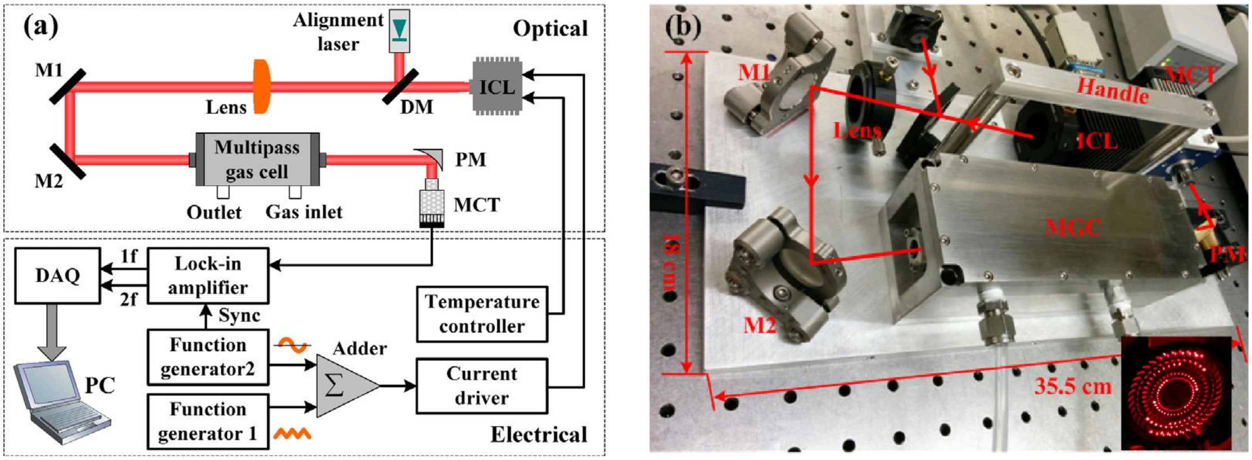

Figure 2. (a) Schematic of the C_2H_6 sensor based on a multipass gas cell and a 3.337 µm CW, TEC ICL excitation source. ICL: interband cascade laser; DM: dichroic mirror; M: plane mirror; PM: parabolic mirror; MCT detector: mercury-cadmium-telluride detector; (b) Photo and physical dimensions of the compact sensor platform.

The ICL current and temperature were controlled using a commercial current driver (Thorlabs, model LDC202C) and a temperature controller (Wavelength Electronics, model LFI-3751), respectively. Two electrical signals that included a triangular signal (0.3 Hz, 0.2 V_{pp}) generated by a function generator 1 and a sinusoidal wave (5 kHz, optimized amplitude of 0.026 V, see Section 2.3) from function generator 2 were added and applied to the current driver to scan and modulate the ICL wavelength. A lock-in amplifier (LIA, Signal Recovery, model 7265) was used to demodulate the signal from the MCT detector by means of a synchronization signal from function generator 2, and both $1f$ and $2f$ harmonic signals were recorded at the LIA output. A data acquisition card (National Instrument, model USB-6356) was used to acquire the $1f$ and $2f$ spectra from the LIA for $2f$-WMS and $2f/1f$ measurements. In addition, a compact, oil-free vacuum pump (Knf Neuberger Inc., model N 813.5 ANE/AF) and a pressure controller (MKS Instruments, Inc., Type 649) were used to pump gas into the MPGC and to control the gas pressure inside the cell, respectively.

2.3. ICL characterization and optimization

The ICL has a wavelength of 3.337 µm in order to target the C_2H_6 absorption line at ~2996.88 cm^{-1}. The Nanoplus TO66-mounted ICL (physical size: $5 \times 5 \times 5$ cm^3) can be operated at temperatures between 5°C and 15°C without forced air or water cooling. A Fourier transform infrared (FTIR) spectrometer (Thermo Scientific, model Nicolet 8700) and a power meter (Ophir Optoelectronics, model 3A) were employed to measure the ICL emission wavelength and power, respectively, at different driving currents. The measured I–V (current-voltage) and P-I (power-current) curves are show in Fig. 3(a). The maximum measured optical power was ~10.5 mW when the ICL was operated at a temperature of 10°C and an injection current of 55 mA. The emission wavenumber can be tuned from 2994.2 cm^{-1} to 3002.7 cm^{-1}, as depicted in Fig. 3(b). The current and temperature wavelength-tuning coefficients for this ICL were experimentally determined to be –0.1415 cm^{-1}/mA and –0.3014 cm^{-1}/°C. An ICL injection current of 47 mA and a 10°C operating temperature were selected for C_2H_6 concentration measurements at the interference-free absorption line of 2996.88 cm^{-1}.

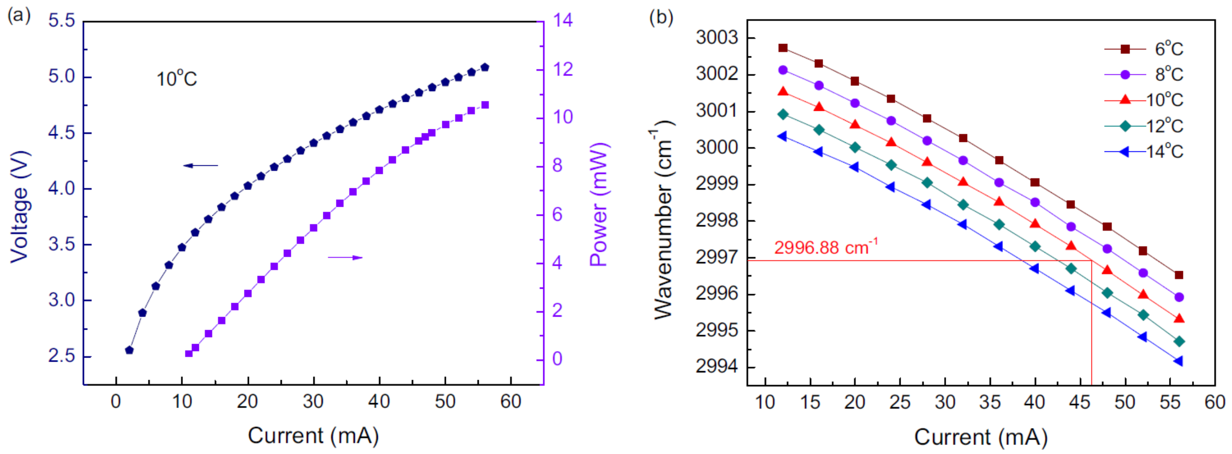

Figure 3. Measured ICL output power and spectral tuning results for the 3.34 µm CW TEC ICL at different operating temperatures and injection currents. (a) L-I-V curve for the laser operating at 10°C. (b) Emission wavenumber plots for different ICL temperatures and driving currents.

To optimize the sensor performance, both the gas pressure and the wavelength modulation depth (denoted by Δv) must be appropriately chosen to achieve the highest 2*f* signal. For this purpose, a certified standard gas cylinder containing 1.14 ppm C_2H_6 balanced by ultra-high purity (UHP) N_2 was employed for the optimization of the C_2H_6 sensor system. Since the developed sensor will be primarily used for atmospheric C_2H_6 detection, low-cost N_2 was chosen as the balance gas, which has a molecular weight similar to air. For each individual pressure ranging from 50 Torr to 200 Torr, the 2*f* signals were recorded with different modulation amplitudes, as depicted in Fig. 4. The modulation amplitude curve as a function of modulation depth is also plotted in Fig. 4. The results illustrate that the maximum C_2H_6 2*f* signal is achieved at a pressure of 200 Torr and a modulation depth of 0.142 cm^{-1} which is based on the measured DC tuning coefficient. However, taking into account the interference from the CH_4 absorption line mentioned previously in Section 2.1 (see Fig. 1), the most suitable pressure and modulation depth are 100 Torr and 0.074 cm^{-1}, respectively, corresponding to an amplitude of the modulation signal of ~0.026 V. The selected absorption line width (γ) is ~0.048 cm^{-1} based on the HITRAN data base and an optimized modulation coefficient of $\Delta v/\gamma = 1.58$ was achieved.

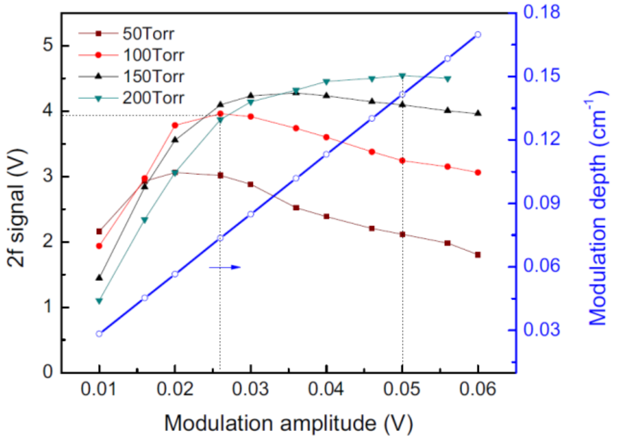

Figure 4. Measured amplitude of the 2f signal and the modulation depth as a function of the modulation amplitude for a dry 200 ppb C_2H_6:N_2 mixture at four different pressure values.

3. Sensor performance assessment using 2*f*-WMS and 2*f*/1*f*-WMS modulation

3.1. Experimental details

For both 2*f*-WMS and 2*f*/1*f*-WMS detection techniques, the driving current and laser temperature were set to 47 mA and 10°C for tuning the ICL wavelength to be centered at 2996.88 cm^{-1}. The pressure in the MPGC was set to 100 Torr. The scan signal used a triangular signal with a frequency of 0.3 Hz and a peak-to-peak amplitude of 200 mV, and the modulation signal employed a sinusoidal signal with a frequency of 5 kHz and an amplitude of 0.026 V. The sensitivity of the lock-in amplifier was set to 50 mV, and the integration time to 10 ms. The generated 1*f* and 2*f* signals are sent to a DAQ card for data sampling. The sampling rate of the DAQ card was set to be 1 kHz, and as a result, each triangular period (including two C_2H_6 spectra) contains 3333 data points. Data sampling was triggered by the triangular-wave scan signal to obtain the position of the peak value of the 2*f* signal during a scan (denoted by max(2*f*)), as depicted in Fig. 5(a)) as well as the position of the mean value of 1*f* signal (denoted by mean(1*f*), as depicted in Fig. 5(b)). The mean(1*f*) value represents the average power of the laser, which can be used for minimizing the drift of the laser power and thus enhancing the sensor system stability [29]. Both the max(2*f*) and mean(1*f*) data were recorded by the computer for subsequent processing and analysis.

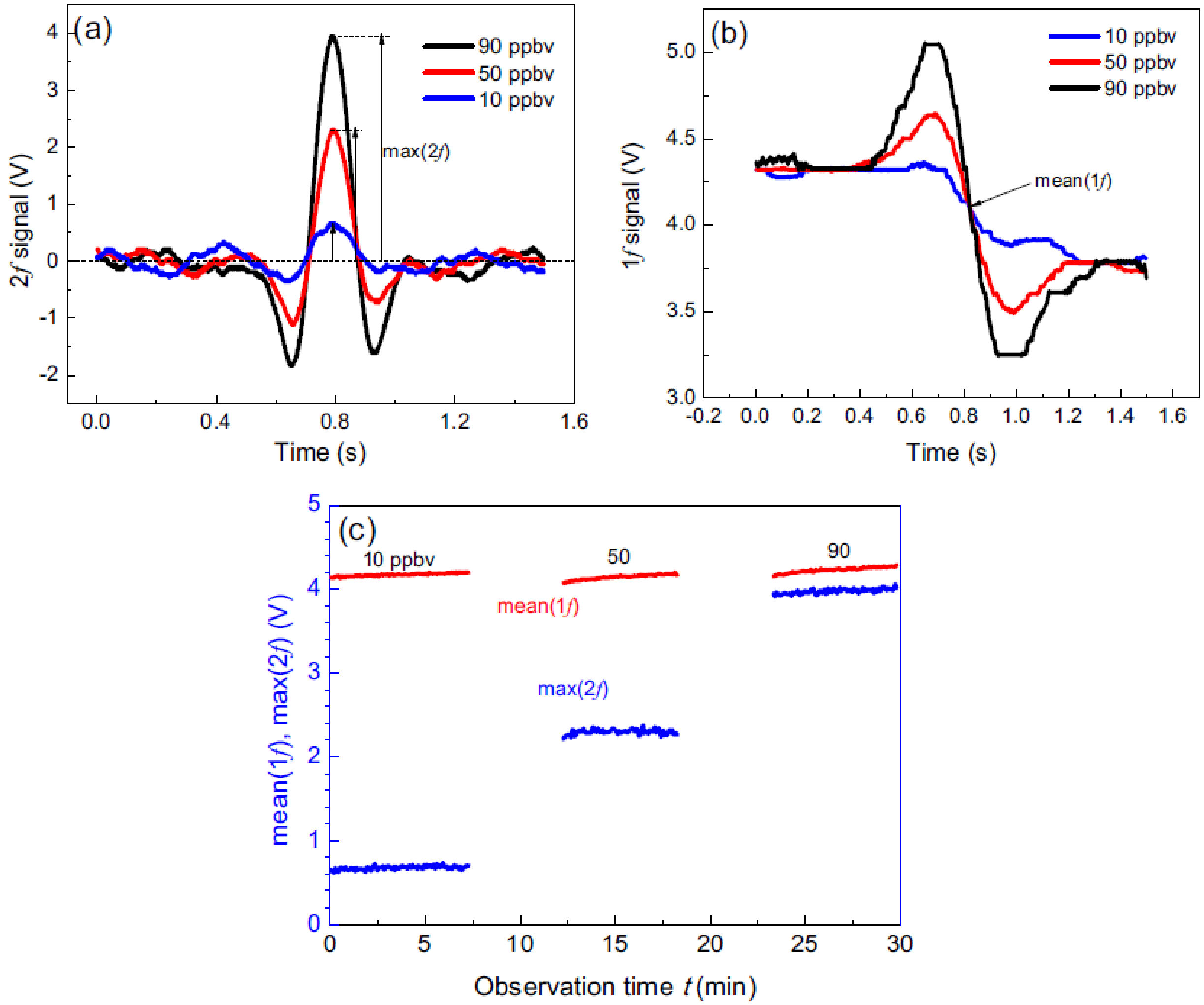

Figure 5. Measured (a) 2f and (b) 1f waveforms for C2H6 concentration levels of 90, 50, and 10 ppbv. (c) Max(2f) and mean(1f) plots versus observation time for concentrations of <90, 50, and 10 ppbv C_2H_6.

C_2H_6 samples with different concentration levels (0–100 ppb) were prepared with a gas dilution system (Environics Inc., Series 4040). The 2*f* and 1*f* waveforms at concentration levels of 10, 50 and 90 ppb are shown in Fig. 5(a) and (b), respectively. In Fig. 5(a), the value of max(2*f*) increases as the concentration levels increase, due to the increased absorption at the peak absorption wavelength. In Fig. 5(b), the value of mean(1*f*) remains constant for the three selected concentrations. However, due to ICL power variations, both values will change for relatively long observation periods, as shown in Fig. 5(c). Furthermore, the three pairs of curves show the same variation trend. Hence, the ratio of max(2*f*)/mean(1*f*) can been used to reduce the effect of the ICL power drift.

3.2. Calibration and data-fitting

Ten C_2H_6 samples covering a concentration range from 10 to 100 ppbv spaced 10 ppbv apart were prepared with the standard gas generator described in Section 3.1. The generated gas samples were pumped into the MPGC. Fig. 6(a) shows the measured value of max(2*f*) and the ratio of max(2*f*)/mean(1*f*) versus the calibration time *t*. Each sample was tested for ~7 min. The ratio of max(2*f*)/mean(1*f*) is more stable compared to max(2*f*) due to eliminating ICL power variations. The measured data of max(2*f*) and max(2*f*)/mean(1*f*) for each concentration were averaged and plotted as a function of the nominal concentration as shown in Fig. 6(b). A linear relation was observed between max(2*f*) and *C* and also between max(2*f*)/mean(1*f*) and *C* is given by:

$$C = 24.26928\max(2f) - 6.62283$$

(1)

$$C = \frac{103.99425\max(2f)}{\mathrm{mean}(1f)} - 7.88507$$

(2)

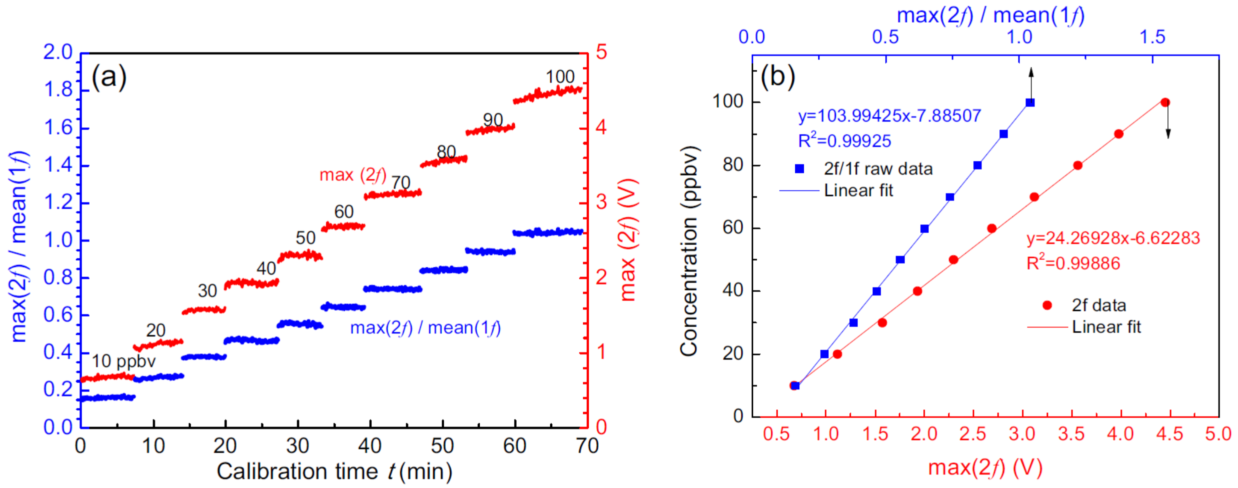

Figure 6. (a) Measured curves of max(2f) and max(2f)/mean(1f) versus calibration time t for 10, 20, 30, 40, 50, 60, 70, 80, 90, 100 ppbv C_2H_6 concentration levels. (b) Experimental dots and fitting curve of both max(2f) versus C_2H_6 concentration and max(2f)/mean(1f) versus C_2H_6 concentration levels.

In Eqs. (1) and (2), due to data-fitting errors, the intercepts of the two curves is not zero. Eqs. (1) and (2) with the measured data of mean(1*f*) and max(2*f*) will be used to determine the C_2H_6 concentration levels.

3.3. Stability

Initially, C_2H_6 measurements with zero gas were performed over a period of ~2 h, and the measured concentrations using both 2*f*-WMS and 2*f*/1*f*-WMS techniques were recorded. An Allan variance is utilized to analyze the stability and the minimum detection limit (MDL) for the two techniques. Fig. 7(a) exhibits the measured concentration versus time *t* and the Allan deviation as a function of the integration time *t* with the 2*f*-WMS technique. The plot indicates that the MDL is ~1.19 ppbv for a 4 s measurement time, and also shows an optimum integration time of 108 s corresponding to a MDL of ~299 pptv. The decreasing red solid line, which is proportional to $(1/\tau)^{1/2}$, indicates that the theoretical expected behavior of a system is dominated by white noise. For the 2*f*/1*f*-WMS technique, the Allan deviation as a function of integration time *t* is shown in Fig. 7(b). The MDL is ~1.05 ppbv for a 4 s measurement time. The Allan plot yields an optimum integration time of ~208 s with an MDL of 239 pptv, which is better than the MDL when using the 2*f*-WMS technique. Hence, the C_2H_6 sensor system stability was improved by means of the 2*f*/1*f*-WMS technique.

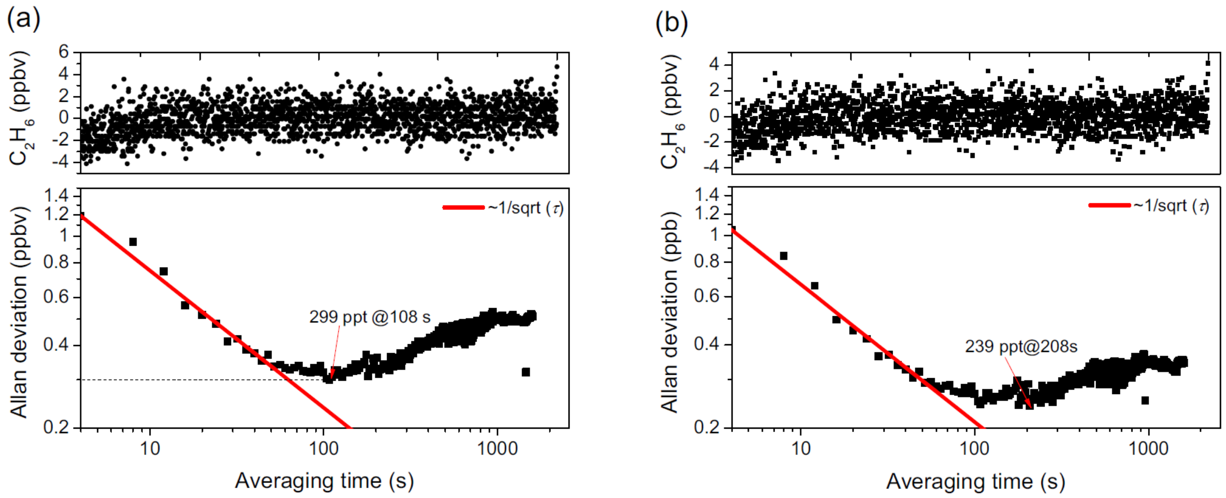

Figure 7. Measured concentration for 0 ppbv C_2H_6 concentration, versus time t and the Allan deviation as a function of integration time t, (a) 2f-WMS technique, (b) 2f/1f-WMS technique.

3.4. Response time

A 'Y' feed line with two entrance ports and one exit port, as shown in Fig. 8(a) was implemented in order to determine the response time. The exit port was connected to the MPGC through a pressure controller. One entrance port was connected to the gas dilution system, through which the prepared gas sample was supplied and the second entrance port was connected to the N_2 cylinder. The two entrance ports could be switched "on" or "off" by two needle valves for the response time tests. With such a measurement scheme, the dynamic PID control process for the gas dilution system does not require to be considered, and the response time is determined by gas flow and cell volume. The measurement results are shown in Fig. 8(b) which indicate a 10–90% rise time and the 90-10% fall time of ~64 and ~48 s, respectively.

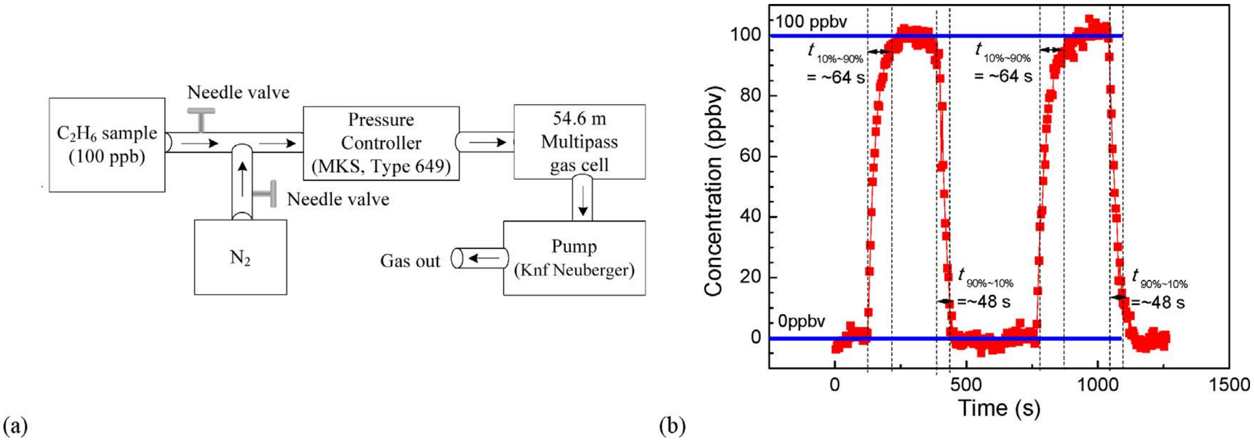

Figure 8. (a) Schematic of a vacuum 'Y' feed line with two entrance ports and one exit port. (b) Response time measurement results by varying C_2H_6 concentration levels between 0 and 100 ppbv.

3.5. Dynamic measurements

The dynamic performance of the sensor was tested next. The output port of the gas dilution system was connected directly to the MPGC via the pressure controller. As shown in Fig. 9, the total mea-surement time was 600 s. The C_2H_6 concentration initially changes from 0 ppbv to 50 ppbv, then decreases to 20 ppbv, and finally increases to 90 ppbv. The concentration level rises sharply, which implies that the sensor response time is shorter than the dynamic PID adjustment time. As the concentration increases, it takes more time for sample preparation and stabilizing the concentration levels. It was shown that the detection results of all samples were equal to the standard values, which illustrates an acceptable detection performance of the reported C_2H_6 sensor system. Furthermore, there is no apparent difference between the 2*f*-WMS technique and 2*f*/1*f*-WMS technique because of the short observation time of each sample.

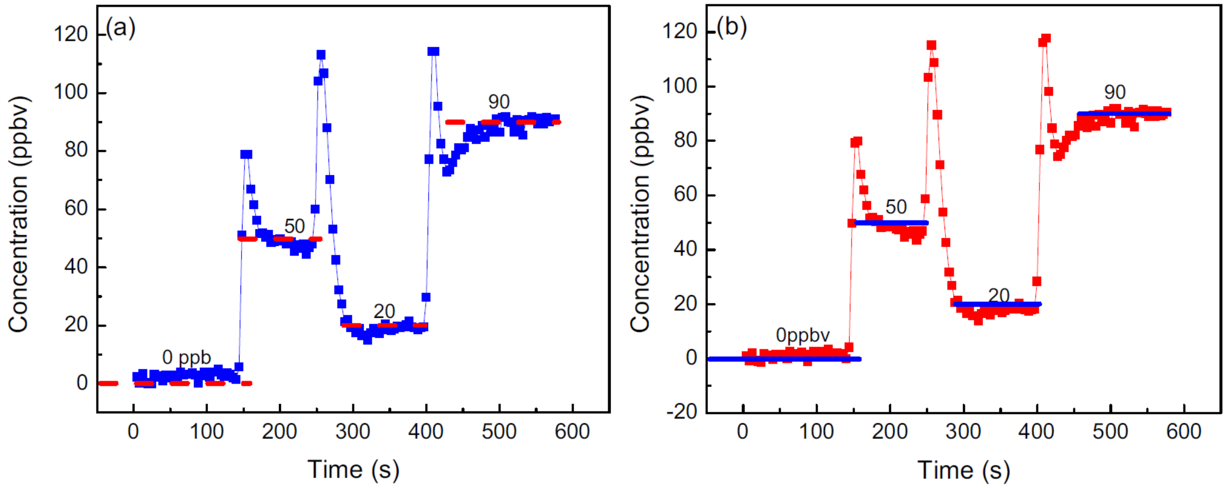

Figure 9. Dynamic measurements of the C_2H_6 sensor using (a) 2f-WMS technique and (b) 2f/1f-WMS technique, when C_2H_6 concentration levels initially change from 0 ppbv to 50 ppbv, then decrease to 20 ppbv, and finally increase to 90 ppbv.

4. Conclusions

In this paper, we reported the design and performance of a mid-infrared C_2H_6 sensor based on a compact optical platform and a CW, DFB, TEC ICL. A C_2H_6 sensor system with a physical size of 35.5 × 18 × 12.5 cm^3 was implemented, consist-ing of an ICL, a MCT detector, mirrors, and a MPGC with a physical size of 17 × 6.5 × 5.5 cm^3. The ICL with a wavelength of ~3.34 µm combined with 2*f*-WMS and 2*f*/1*f*-WMS was applied to an interference-free absorption line located at 2996.88 cm^{-1} at a pressure of 100 Torr in order to achieve C_2H_6 measurements at ppb-level concentration levels. The optimum modulation depth was 0.074 cm^{-1}. The sensor performance was improved by reducing the effect of ICL power drift by means of the 2*f*/1*f*-WMS technique. The MDL is ~1.19 parts per billion (ppbv) for 2*f*-WMS and ~1.05 ppbv for 2*f*/1*f*-WMS techniques, respectively with a measurement time of 4 s. Furthermore, the sensor stability can be improved from 299 pptv (@108 s for the 2*f*-WMS method) to 239 pptv (@208 s using the 2*f*/1*f*-WMS method). The detection sensitivity and stability of the reported C_2H_6 sensor system can be further improved by a redesign of the optical sensor components to further suppress optical fringes by implementing line-locking functionality which requires addition of a reference channel.

Acknowledgements

Chunguang Li acknowledges support by China Scholarship Council (Grant No. 201406170107). Frank Tittel acknowledges sup-port by the National Science Foundation (NSF) ERC MIRTHE award, a Robert Welch Foundation Grant C-0586, a NSF Phase II SBIR (Grant No. IIP-1230427) and by ARPA-E under award # DE AR0000548 and DE-AR0000545. Chuantao Zheng acknowledges the support by China Scholarship Council (Grant No. 201506175025), the National Natural Science Foundation of China (Grant No. 61307124), and the Changchun Municipal Science and Technology Bureau (Grant No. 14KG022). Lei Dong acknowledges support by National Natural Science Foundation of China (Grant Nos. 61575113 and 61275213).

References

[1] I.J. Simpson, F.S. Rowland, S. Meinardi, D.R. Blake, Influence of biomass burning during recent fluctuations in the slow growth of global tropospheric methane, Geophys. Res. Lett. 33 (2006) L22808.

[2] Y. Xiao, J.A. Logan, D.J. Jacob, R.C. Hudman, R. Yantosca, D.R. Blake, Global budget of ethane and regional constraints on U.S. sources, J. Geophys. Res. 113 (2008) D21306.

[3] L.C. Thomson, B. Hirst, G. Gibson, S. Gillespie, P. Jonathan, K.D. Skeldon, M.J. Padgett, An improved algorithm for locating a gas source using inverse methods, Atmos. Environ. 41 (2007) 1128–1134.

[4] G. Etiope, P. Ciccioli, Earth’s degassing: a missing ethane and propane source, Science 323 (5913) (2009) 478.

[5] P. Paredi, S.A. Kharitonov, P.J. Barnes, Elevation of exhaled ethane concentration in asthma, Am. J. Respir. Crit. Care Med. 162 (2000) 1450–1454.

[6] B.K. Puri, B.M. Ross, I.H. Treasaden, Increased levels of ethane a non-invasive, quantitative, direct marker of n-3 lipid peroxidation, in the breath of patients with schizophrenia, Prog. Neuropsychopharmacol. Biol. Psychiatry 32 (2008) 858–862.

[7] K.D. Skeldon, L.C. McMillan, C.A. Wyse, S.D. Monk, G. Gibson, C. Patterson, T. France, C. Longbottom, M.J. Padgett, Application of laser spectroscopy for measurement of exhaled ethane in patients with lung cancer, Respir. Med. 100 (2006) 300–306.

[8] J.A. Silver, Frequency-modulation spectroscopy for trace species detection: theory and comparison among experimental methods, Appl. Opt. 31 (6) (1992) 707–717.

[9] P. Werle, A review of recent advances in semiconductor laser based gas monitors, Spectrochim. Acta A 54 (1998) 197–236.

[10] S. Schilt, L. Thévenaz, P. Robert, Wavelength modulation spectroscopy: combined frequency and intensity laser modulation, Appl. Opt. 42 (33) (2003) 6728–6738.

[11] G. Wysocki, Y. Bakhirkin, S. So, F.K. Tittel, C.J. Hill, R.Q. Yang, M.P. Fraser, Dual interband cascade laser based trace-gas sensor for environmental monitoring, Appl. Opt. 46 (33) (2007) 8202–8210.

[12] M.N. Fiddler, I. Begashaw, M.A. Mickens, M.S. Collingwood, Z. Assefa, S. Bililign, Laser spectroscopy for atmospheric and environmental sensing, Sensors 9 (2009) 10447–10512.

[13] R.F. Curl, F. Capasso, C. Gmachl, A.A. Kosterev, B. McManus, R. Lewicki, M. Pusharsky, G. Wysocki, F.K. Tittel, Quantum cascade lasers in chemical physics, Chem. Phys. Lett. Front. Artic. 487 (2010) 1–18.

[14] M.R. McCurdy, Y. Bakhirkin, G. Wysocki, R. Lewicki, F.K. Tittel, Recent advances of laser – spectroscopy-based techniques for applications in breath analysis, J. Breath Res. 1 (2007) 014001.

[15] T.H. Risby, F.K. Tittel, Current status of midinfrared quantum and interband cascade lasers for clinical breath analysis, SPIE Opt. Eng. 49 (11) (2010) 111123.

[16] J.H. Shorter, D.D. Nelson, J.B. McManus, M.S. Zahniser, D.K. Milton, Multicomponent breath analysis with infrared absorption using room-temperature quantum cascade lasers, IEEE Sens. J. 10 (1) (2010) 76–84.

[17] J.H. Shorter, D.D. Nelson, J.B. McManus, M.S. Zahniser, S.R. Sama, D.K. Milton, Clinical study of multiple breath biomarkers of asthma and COPD (NO CO_2, CO and N_2O) by infrared laser spectroscopy, J. Breath Res. 5 (2011) 037108.

[18] M.R. McCurdy, A. Sharafkhaneh, H. Abdel-Monem, J. Rojo, F.K. Tittel, Exhaled nitric oxide parameters and functional capacity in chronic obstructive pulmonary disease, J. Breath Res. 5 (2011) 016003.

[19] K.R. Parameswaran, D.I. Rosen, M.G. Allan, A.M. Ganz, T.H. Risby, Off-axis integrated cavity output spectroscopy with a mid-infrared interband cascade laser for real-time breath ethane measurements, Appl. Opt. 48 (4) (2009) B73–B79.

[20] D. Halmer, S. Thelen, P. Hering, M. Murtz, Online monitoring of ethane traces in exhaled breath with a difference frequency generation spectrometer, Appl. Phys. B 85 (2006) 437–443.

[21] G. Wysocki, A.A. Kosterev, F.K. Tittel, Spectroscopic trace-gas sensor with rapidly scanned wavelengths of a pulsed quantum cascade laser for in situ NO monitoring of industrial exhaust systems, Appl. Phys. B 80 (2005) 617–625.

[22] M. Lewander, Z.G. Guan, L. Persson, A. Olsson, S. Svanberg, Food monitoring based on diode laser gas spectroscopy, Appl. Phys. B 93 (2008) 619–625.

[23] J. Chen, S. So, H. Lee, M.P. Fraser, R.F. Curl, T. Harman, F.K. Tittel, Atmospheric formaldehyde monitoring in the Greater Houston area in 2002, Appl. Spectrosc. 58 (2) (2004) 243–247.

[24] M. Angelmahr, A. Miklos, P. Hess, Photoacoustic spectroscopy offormaldehyde with tunable laser radiation at the parts per billion level, Appl.Phys. B 85 (2-3) (2006) 285–288.

[25] J. Li, U. Parchatka, H. Fischer, A formaldehyde trace gas sensor based on athermoelectrically cooled CW-DFB quantum cascade laser, Anal. Methods 6(15) (2014) 5483–5488.

[26] J.H. Miller, Y.A. Bakhirkin, T. Ajtai, F.K. Tittel, C.J. Hill, R.Q. Yang, Detection offormaldehyde using off-axis integrated cavity output spectroscopy with aninterband cascade laser, Appl. Phys. B 85 (2-3) (2006) 391–396.

[27] K. Krzempek, M. Jahjah, R. Lewicki, P. Stefanski, S. So, D. Thomazy, F.K. Tittel,CW DFB RT diode laser-based sensor for trace-gas detection of ethane using anovel compact multipass gas absorption cell, Appl. Phys. B 112 (2013)461–465.

[28] K. Krzempek, R. Lewicki, L. Naehle, M. Fischer, J. Koeth, S. Belahsene, Y.Rouillard, L. Worschech, F.K. Tittel, Continuous wave, distributed feedbackdiode laser based sensor for trace-gas detection of ethane, Appl. Phys. B 106(2012) 251–255.

[29] G.B. Rieker, J.B. Jeffries, R.K. Hanson, Calibration-free wavelength-modulationspectroscopy for measurements of gas temperature and concentration inharsh environments, Appl. Opt. 48 (29) (2009) 5546–5560.

[30] L.J. Lan, Y.J. Ding, Z.M. Peng, Y.J. Du, Y.F. Liu, Calibration-free wavelengthmodulation for gas sensing in tunable diode laser absorption spectroscopy,Appl. Phys. B 117 (2014) 1211–1219.

[31] L.S. Rothman, I.E. Gordon, Y. Babikov, A. Barbe, D. Chris Benner, P.F. Bernath,M. Birk, L. Bizzocchi, V. Boudon, L.R. Brown, A. Campargue, K. Chance, E.A.Cohen, L.H. Coudert, V.M. Devi, B.J. Drouin, A. Fayt, J.-M. Flaud, R.R. Gamache,J.J. Harrison, J.-M. Hartmann, C. Hill, J.T. Hodges, D. Jacquemart, A. Jolly, J.Lamouroux, R.J. LeRoy, G. Li, D.A. Long, O. Lyulin, C. Mackie, S.T. Massie, S.Mikhailenko, H.S. Müller, O. Naumenko, A. Nikitin, J. Orphal, V.I. Perevalov, A.Perrin, E.R. Polovtseva, C. Richard, M.A.H. Smith, E. Starikova, K. Sung, S.Tashkun, J. Tennyson, G.C. Toon, Vl G. Tyuterev, G. Wagner, The HITRAN 2012molecular spectroscopic database, J. Quant. Spectrosc. Radiat. Transfer 130(2013) 4–50.